ChemPubSoc Europe

DOI: 10.1002/chem.201404309

CHEMISTRY
A European Journal
Full Paper

Graphene | *Hot Paper*

Strong Interplay between the Electron Spin Lifetime in Chemically Synthesized Graphene Multilayers and Surface-Bound Oxygen

Bálint Náfrádi,*[a] Mohammad Choucair,[b] Peter D. Southon,[b] Cameron J. Kepert,[b] and László Forró[a]

Abstract: The electron spin lifetime in an assembly of chemically synthesized graphene sheets was found to be extremely sensitive to oxygen. Introducing small concentrations of physisorbed O_2 onto the graphene surface reduced the exceptionally long 140 ns electron spin lifetime by an order of magnitude. This effect was completely reversible: Removing the O_2 by using a dynamic vacuum restored the spin lifetime. The presence of covalently bound oxygen also decreased the electron spin lifetime in graphene, although to a far lesser extent compared to physisorbed O_2. The conduction electrons in graphene were found to play a significant role by counter-balancing the spin depolarization caused by oxygen molecules. Our results highlight the importance of chemical environment control and device packing in practical graphene-based spintronic applications.

1. Introduction

Spintronic technologies represent a paradigm shift in the field of nano-electronics as they utilize electron spin in addition to charge for device functionality. Graphene has been proposed as an ideal material for spintronic and spin quantum computing applications due to the expected long intrinsic spin lifetimes (T_S) arising from the small spin-orbit coupling of carbon atoms and the weak hyperfine interactions resulting from the absence of nuclear spins for the main ^{12}C isotope. However, the current achievable electron spin lifetime (T_S) values for graphene determined by spin transport experiments are unexpectedly short: They range between 0.2 to 2.3 ns.[1] The T_S values in spin transport measurements for graphene remain contentious as identifying the intrinsic T_S as spin transport devices arrives at notable drawbacks with the use of traditional metallic ferromagnetic contacts.[2] It has been proposed that sample preparation has an important effect on the measured T_S.[1b] Alternative scenarios to explain unexpectedly small T_S found in graphene have included effects of substrate,[3] impurities,[4] finite-sized flakes,[5] and ripples.[6]

We have recently employed the contactless spectroscopic technique of electron spin resonance (ESR) to overcome the effects of substrate and contact contributions to identify a remarkably long T_S of 65 ns in high purity chemically synthesized graphene.[7] This earlier study unambiguously demonstrated that intrinsic T_S of itinerant conduction electrons of graphene can be as long as 65 ns, thus the experimental T_S obtained in spin transport is reduced by extrinsic factors.

To pinpoint the key parameters responsible for the experimentally observed short T_S is the motivation of our present study. To this end, we directly employ a substrate-free self-supported graphene material, free of metallic impurities, to investigate the intrinsic spin dynamics and the effect of oxygen interactions with graphene. The extended three-dimensional network of graphene represents a model system, displaying both locally high quality graphene and disorder on a large scale[7–8] that allows fine-tuning of T_S over a broad range due to this materials unprecedentedly long intrinsic T_S. We demonstrate that the presence of physisorbed and chemisorbed oxygen molecules reduces the spin lifetime of graphene by more than an order of magnitude. Nanometer differences in oxygen-to-carbon spin distances are sufficient to drastically alter the electron spin lifetime.

ESR is a powerful probe of local electron environment ideally suited to distinguish the specific atomic nature of point defects and various localized and itinerant spin states in carbon materials.[9] ESR allows for the separate acquisition of signals originating from various regions within a material.[10] These regions can be affected by the presence of various gases.[11] For example, the reversible change of ESR signal intensity upon O_2 exposure suggests potential sensory applications.[11c] However, for such applications to eventuate there is a demand for detailed investigations into the microscopic mechanism of the O_2–graphene interaction process and its impact on graphene spin lifetime and spintronic applicability.

In the case in which molecular oxygen interacts with the graphene surface, ESR can be used to deduce important

[a] *Dr. B. Náfrádi, Prof. L. Forró*
Institute of Physics of Complex Matter EPFL
Lausanne (Switzerland)
E-mail: nafradi@yahoo.com

[b] *Dr. M. Choucair, Dr. P. D. Southon, Prof. C. J. Kepert*
School of Chemistry
The University of Sydney
Sydney 2006 (Australia)

Supporting information for this article is available on the WWW under http://dx.doi.org/10.1002/chem.201404309.

information arising from (but not limited to) a few possible scenarios: 1) If O_2 is significantly close to the surface, the line width of ESR signal would broaden (beyond detection limits) and appear as a reduction in susceptibility; 2) when O_2 is sufficiently far removed from the surface, conduction electrons average the entire signal and a signal with Lorentzian peak characteristics would then be observed; and 3) those carbon spins that are somewhere between the limits imposed by O_2 in scenarios (1) and (2) may be revealed by contributions to a signal with a distorted Lorentzian line shape. This is because O_2 gas is paramagnetic with spin-1 magnetic moment. By tuning the O_2 concentration and manipulating the efficiency of the motional narrowing caused by conduction, electrons estimations of the O_2–carbon spin distances may be obtained. However, distinguishing these scenarios inherently relies on the use of high quality graphene materials that demonstrate long electron spin lifetime.

2. Experimental

2.1 Synthesis

The assembly of graphene sheets was obtained by a previously reported solvothermal synthesis pathway.[7–8] To summarize, propanol was used as the alcohol feedstock for the solvothermal reaction with sodium metal at 493 K for 72 h. The term "solvothermal" denotes conditions involving reactions performed at a temperature above the boiling point of a solvent in a closed reaction vessel. The solvothermal reaction yielded a solid product, which was rapidly pyrolized in air, resulting in a moderately oxidized graphene material. The resulting material was washed with water, then with acidified ethanol (2 M hydrochloric acid in ethanol, 1:4 v/v ratio), and filtered under dynamic vacuum before drying in a vacuum oven at 473 K for 1 h.

2.2 Characterization

Transmission electron microscopy (TEM) was performed on a JEOL3000F operated at an acceleration voltage of 300 kV. The graphene sample was prepared by sonication for a few minutes in ethanol, then dropped directly onto a carbon-coated copper TEM grid and after allowed to air dry.

Raman spectroscopy was performed using Argon 514 nm excitation laser on a Renishaw Raman inVia Reflex with a notch and edge filter cut-off of 100 cm^{-1} (10% laser power, 10 s acquisition, 10 acquisitions, 50× objective) and a spectral resolution of $\approx$1.4 cm^{-1}. A small amount of sample was shaken in ethanol before dropping onto a stainless steel plate and allowed to air dry prior to analysis.

Gas adsorption isotherms were measured with an IGA-002 gravimetric adsorption instrument (Hiden–Isochema). Approximately 44 mg of graphene was loaded into a stainless steel basket and sealed in a stainless steel microbalance chamber. The chamber was evacuated, and heated to 715 K for 12 h before cooling. Isotherms were measured by pressurizing the sample chamber with a set pressure of gas, monitoring the mass for a minimum time to reach equilibrium, before increasing the pressure to the next programmed point. The sample temperature was maintained at (298.1 $\pm$ 0.1) K. The gases were supplied at 99.99% purity.

X-ray photoelectron spectroscopy (XPS) measurements were conducted using an ESCALAB250Xi instrument manufactured by Thermo Scientific, UK. The background vacuum was below 2×10^{-9} mbar. Monochromated $Al_{K\alpha}$ (1486.68 eV) with a power of 156 W (12 mA and 13 kV) and a spot size of 500 μm was used. The photoelectron take-off angle was 90° and the pass energy was 20 eV for high-resolution surface region scans. Under the surface region scan conditions, a spectral resolution of 0.59 eV (full width at half maximum) was achieved. The spectrometer was calibrated using Au $4f_{7/2}=83.96$ eV, Ag $3d_{5/2}=368.21$ eV, Cu $2p_{3/2}=932.62$ eV with a C 1s binding reference of 285.00 eV for adventitious hydrocarbon. The material was pressed into a disc and placed onto a Cu heating stage for analysis. Curve fitting was performed using the Scienta ESCA300 data-system software. This describes each of the components of a complex envelope as a Gaussian–Lorentzian sum function. The curve fit is guided using chemical and physical knowledge, rather than allowing the algorithms to produce what may be a good mathematical fit, but lacking physical meaning.

ESR spectroscopy in the 9.4–420 GHz frequency range was performed. The temperature was varied in the range 2–300 K. At 9.4 GHz a commercial spectrometer was used. In the millimeter wave range, experiments were carried out on a home-made 105–420 GHz quasi optical spectrometer.[12] To enhance sensitivity, first-derivative-absorption spectra were detected by a lock-in technique through applying sinusoidal modulation of the externally applied magnetic field. The incident microwave power as well as the modulation amplitude was cautiously reduced to avoid signal distortion. The ESR line width (ΔH), g-factor, and spin susceptibility (χ), were quantified by least squares fitting of the derivative absorption spectra. The absolute value of χ was determined by a calibrated $CuSO_4{\cdot}5H_2O$ reference sample.[13] The g-factor was determined with the aid of 10 ppm Mn-doped Mn/MgO powder with $g=2.0014$.[14]

3. Results and Discussion

3.1 Gas and vapor sorption, microscopy, Raman spectroscopy, and X-ray photoelectron spectroscopy analysis

First, we characterized the chemical changes in the graphene sample as a function of atmosphere and temperature. TEM images of the graphene material are shown in Figure 1and also the Supporting Information (Figure S1).

According to Ferrari and Robertson,[15] the Raman spectra of the graphene material we employed is best represented by a disordered carbon material between nano-crystalline graphite to low sp^3 amorphous carbon (Figure 2). The Raman spectrum of the graphene material showed a "G band" centered at 1590 cm^{-1} with 91 cm^{-1} full width at half maximum (FWHM), due to the in-plane stretching motion between pairs of sp^2 carbon atoms. The presence of the "D band" centered at

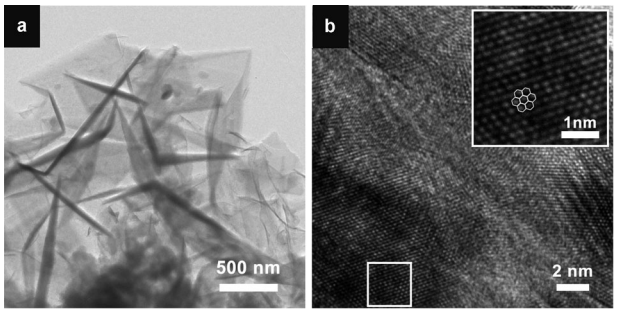

Figure 1. Transmission electron microscopy images of typical regions in the graphene sample a) showing the extended assembly of graphene sheets and b) a high-resolution image of layered graphene sheets with no interplanar correlation. Sheet corrugation was also visible. Inset of (b) shows a magnified region of the hexagonally arranged graphene lattice with hexagons drawn as a guide for the eye.

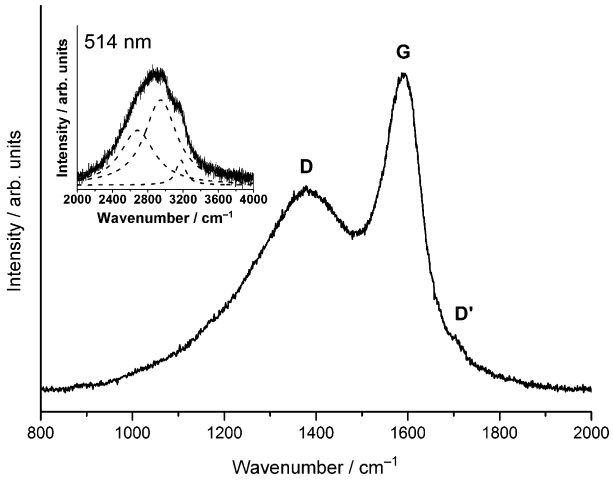

Figure 2. Raman spectra of the as-prepared graphene material. Inset shows the region of second-order peaks.

1381 cm^{-1} with a full width at half maximum (FWHM) of 338 cm^{-1} is believed to be due to a double resonance, and enhanced by edge effects and dangling bonds of the sp^2 carbon sites.[16] The second order peaks are not well defined, but appear as a small modulated bump between 2000 and 3200 cm^{-1} and best represent a multilayer graphitic material.

The intensity ratio of the D band to the G band value, commonly reported as I_D/I_G, was $\approx$0.62, indicating a significant number of defect sites present.[15–16] More generally, and as a first approximation, the Raman spectra of such disordered carbon implied an average inter-defect distance (L_D) of $\approx$1.1 nm, and in terms of defect density (n_D), a number greater than 2.8×10^{13} cm^{-2}.[17] Locally, TEM characterization showed that the in-plane crystalline domains may be inhomogeneous in size resulting in various degrees of local structural disorder within the sp^2 network. Such domains appear within extended micron-sized sheets (contributing to the overall Raman spectra of disordered carbon), and not as amorphous carbon fragments. Consequently, any significant information on the influence of doping[18] and strain[19] on the electronic properties of the graphene material is lost in the background of the Raman spectra of disordered carbon.[15–16] However, from our previous work,[7] we found that the low-temperature metal-like Pauli spin susceptibility arising from this graphene material ($\chi_{Pauli}=3.1\times10^{-7}$ emu g^{-1}) corresponds to carrier densities of approximately 1.44×10^{10} cm^{-2} (assuming linear graphene-like dispersion in the metallic regions), and that the layer coupling strength at 100 K was $\approx$10 meV. Accordingly, either the defective regions of the material do not contribute to the ESR signal, or structural defects do not broaden the ESR signal due to the weak spin-orbit interaction of carbon.

Evacuation of the graphene sample to pressures below 10^{-5} mbar at 296 K resulted in a reduction of $\approx$13 weight percent (wt.%; Figure 3). Since most of the mass loss occurred under relatively mild vacuum, we assume that physisorbed species were removed but not a significant fraction of chemically bound species. Subsequent heating at 715 K under high vacuum for 12 h was sufficient to remove most of the chemically bound molecules from the graphene surface. We performed adsorption–desorption isotherms on the heat-treated graphene at 298 K for the main components of air, N_2 and O_2, H_2O, and CO_2 (Figure 4).

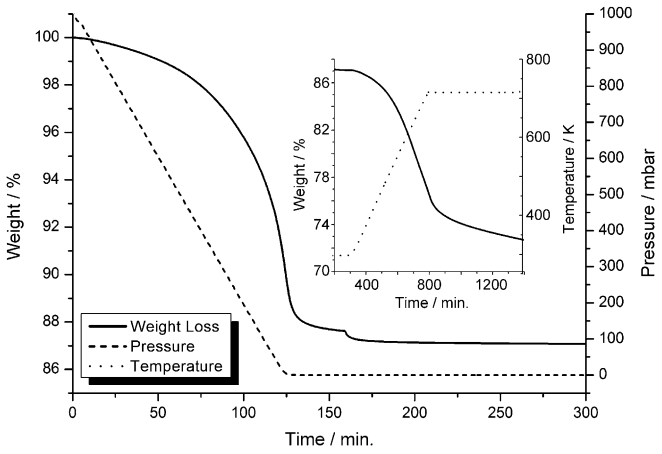

Figure 3. The weight-loss profile of the as-prepared sample with reduction of pressure. The slight kink in the weight loss just after 150 min is due to the start-up of the turbo molecular vacuum pump reducing pressure from 2 to less than 10^{-5} mbar. The inset shows the weight-loss profile during heating to 723 K under high vacuum, in which a further $\approx$15 wt.% was lost.

At 50% relative humidity the graphene sample adsorbed $\approx$10.9 wt.% H_2O. The total adsorption of water at 88% relative humidity in air at 298 K, that is, 28 mbar, reached $\approx$20.7 wt.%. The quantities of adsorbed O_2, N_2, and CO_2 at the partial pressures approximately found in air (212 mbar for O_2, 790 mbar for N_2, 0.4 mbar for CO_2) were 0.38, 0.62, and $\ll$0.05 wt.%, respectively. CO_2, N_2, and H_2O demonstrated largely reversible adsorption behavior. However, the total O_2 uptake was largely irreversible, with approximately two thirds of the oxygen remaining bound upon evacuation. During O_2 adsorption the equilibrium mass at each pressure was not reached even after 2–3 h, so the measured (non-equilibrium) mass at the end the waiting period was used for each point in the isotherm.

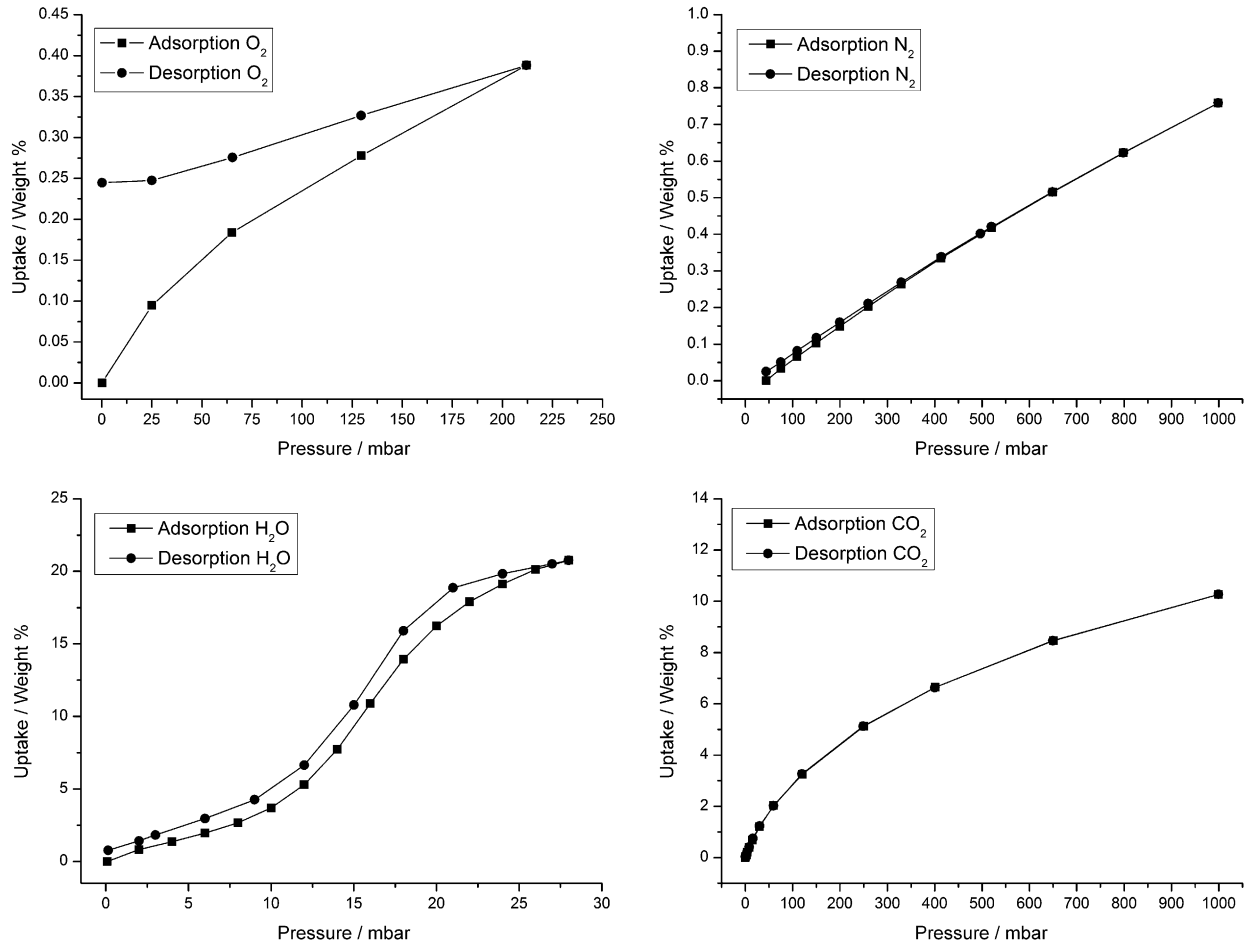

Figure 4. Gas adsorption–desorption isotherms at 298 K for O_2, N_2, H_2O, and CO_2 on graphene.

Further kinetic studies of O_2 sorption revealed two processes occurring at different rates (Figure 5). As O_2 is introduced the initial rapid mass uptake is complete within 2–3 min, typical of the physisorption of gases at room temperature. Beyond this point, there is a slow increase of mass over many hours, which is more characteristic of a process requiring higher activation energy, such as chemical binding or network diffusion. That this second process was not observed for the adsorption of nitrogen or carbon dioxide leads us to believe that it is specific to the gradual chemical oxidation of the graphene surface. The mass gain kinetics for the slow process measured at 65 mbar was fitted to a Linear Driving Force model[20] and the rate constant k was calculated to be (124 ± 3) min, indicating that collection times of longer than 6 h per point would be required to make a reasonable estimate of the equilibrium mass. Note that the measured irreversible oxygen uptake is much less (by more than an order of magnitude) than the initial mass lost during heating.

The water adsorption isotherm indicates that the amount of water adsorbed on the surface of the graphene (and thus the mass lost on evacuation) is highly dependent on the relative humidity in the air. Assuming that the vast bulk of the 13 wt.% mass loss on evacuation is adsorbed water, we estimate that

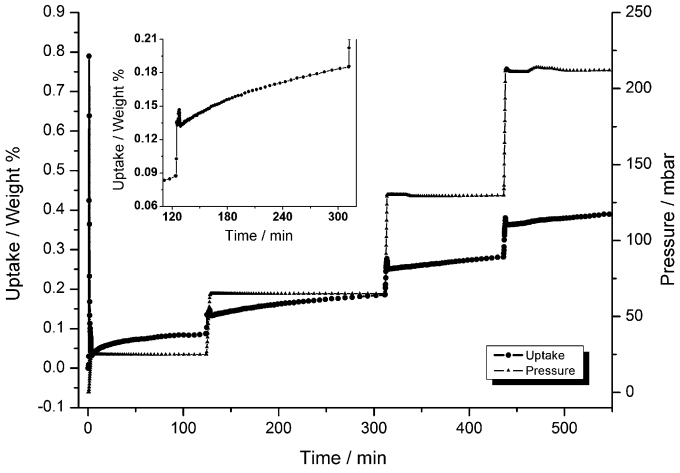

Figure 5. The O_2 uptake at various pressures were collected for a minimum of 2 h yet did not fully reach equilibrium. O_2 adsorption indicates a two-step process involving both fast and slow sorption. The inset shows a magnified region of O_2 adsorption more clearly demonstrating the two-step process: A rapid uptake of O_2 (physisorption) then a very slow uptake (diffusion, physisorption, or chemisorption) over many hours. The spike in the mass reading just after the introduction of O_2 at each pressure is due to the effect of gas turbulence on the microbalance, which takes a few minutes to stabilize.

the relative humidity was approximately 50–55% in the air introduced to the sample.

The composition of the adsorbed surface layer under atmospheric conditions (and 50% relative humidity) was estimated from the pure gas isotherms, neglecting competitive adsorption. The species O_2, N_2, and H_2O were each calculated to exceed the total number of spin = 1/2 paramagnetic centers per gram of the graphene material ($\chi = 3.7\times10^{19}$ spin g^{-1}): $O_2 = 7.3\times10^{19}$, $N_2 = 1.5\times10^{20}$, $H_2O = 3.6\times10^{21}$, and $CO_2 = 3.5\times10^{18}$ molecules g^{-1}. This equates to an approximate ratio of number of guest molecules to spin = 1/2 paramagnetic centers to be 2:1 (O_2), 4:1 (N_2), 100:1 (H_2O), and 1:10 (CO_2).

Weight-loss events when heating to 1070 K were identified using thermogravimetric methods under an atmosphere of ultrapure helium and are reported in the Supporting Information, Figure S2. The removal of adsorbates (solvents, vapors, gases) occurred between 300–430 K and the partial decomposition of the graphene material to CO_2 and CO by the irreversible removal of chemically bound oxygen groups occurred at temperatures exceeding 430 K (Figure 6).[8a] The removal of

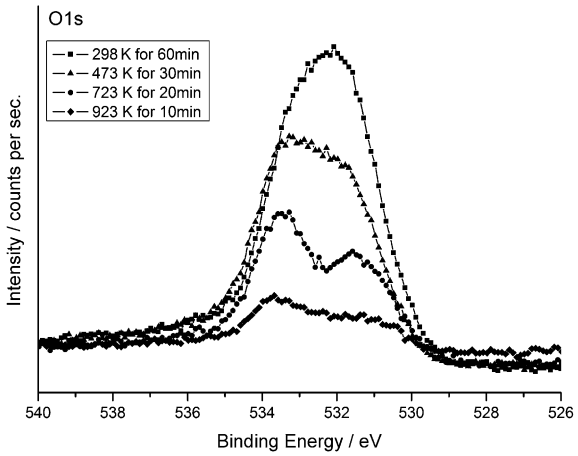

Figure 6. XPS spectra of the core O 1s photoelectron line taken of the as-prepared graphene sample during heating from 298 to 923 K under UHV. The oxygen content chemically attached to the graphene surface was drastically reduced from ≈19 wt.% at 298 K to < 1 wt.% at 923 K over a period of 2 h.

chemically bound oxygen from the surface of the graphene sample was quantitatively monitored in-situ under ultrahigh vacuum (UHV) conditions using XPS, Figure 6.

The oxygen content was found to decrease significantly when heating up to 923 K; a reduction from ≈19 to < 1 wt.%. An estimate of the type of oxygen bound to the carbon was assigned by peak-fitting techniques commonly employed for XPS, which gave approximate quantifications of the chemically bound oxygen environments: O=C of 10.2 wt.% (531.6 eV) and O–C of 8.7 wt.% (533.1 eV) at 298 K under UHV. At 473 K the amount of oxygen left bound as O=C (7.0 wt.%) had been removed significantly more compared to O–C (8.1 wt.%) groups. The peaks appear better resolved after heating at 723 K and the estimated values of chemically bound oxygen reduce to similar quantities: O=C 4.1 wt.% (531.2 eV) and O–C 5.4 wt.% (533.5 eV). It was, however, inappropriate to quantify peak assignments at such low concentrations of oxygen bound (< 1 wt.%) beyond heating at 723 K.

3.2 Electron spin resonance spectroscopy studies

We correlated the results in the above section with spin lifetime changes in the graphene material by means of multi-frequency ESR spectroscopy. At 300 K the 9.4 GHz ESR signal of the as-prepared graphene material had a highly symmetric Lorentzian shape at $g = 2.0137$ position typical of graphitic material,[21] with a line width $\Delta H = 0.41$ mT (the Supporting Information, Figure S3.1 a). A residual non-Lorentzian intensity was also observed from the ESR of the graphene sample. The deviation from the derivative Lorentzian line shape is small with a peak-to-peak magnitude of about 20 times smaller than the signal, which corresponds to a resolved small signal inhomogeneity in the sample of ≈5%. The spin relaxation of the detected signal is largely homogeneous; unresolved inhomogeneity would result in a Gaussian line shape.

From the ESR signal intensity of the as-prepared graphene sample, the spin concentration was calculated[13] and was found to be $\chi = 1.5\times10^{18}$ spin g^{-1} assuming spin = 1/2 paramagnetic moments. It is important to note that the magnitude of the intensity of the ESR signal may be subject to artifacts such as those caused by guest molecule adsorption;[11c] spin magnetic moments may be present although rendered undetectable by ESR[13,22] thus the estimated spin concentrations are lower limits as we show below.

Upon evacuation of the sample overnight in dynamic vacuum of 10^{-5} mbar the ESR signal changed significantly. The *g*-factor remained the same within experimental accuracy, but the ESR line width decreased by more than a factor of 4 and reached $\Delta H = 0.106$ mT. The ESR intensity increased approximately by a factor of 3. The change in ESR line width and intensity upon degassing was completely reversible: Exposing the degassed sample to air immediately broadened the line to recover the original ESR signal. Additionally, the partially degased sample showed slow degradation. The ESR line observed right after sample preparation, presented in Figure 7, over a month timescale transformed back to the as-grown state. We attribute this slow change to the slow surface diffusion of the residual O_2 in excellent agreement with gas absorption results (Figure 5).

The introduction of ultra-pure O_2 gas (at 1 bar) after evacuating the sample also fully restored the ESR line width, however, with an ESR signal intensity half of that observed resulting from air. This loss of signal intensity is in agreement with earlier works,[11c] and demonstrates that a change in signal intensity may be induced by the introduction of O_2 from air. Moreover, our results indicate that the T_S change of graphene is also induced by the graphene–O_2 interaction.

We performed subsequent heat treatments up to 1040 K under dynamic vacuum (typically for 20 min. at each temperature) and measured the ESR at $T = 300$ K after each heat treatment (Figure 7). The *g*-factor was found to be independent of heat treatment. The ESR line width decreased monotonically as

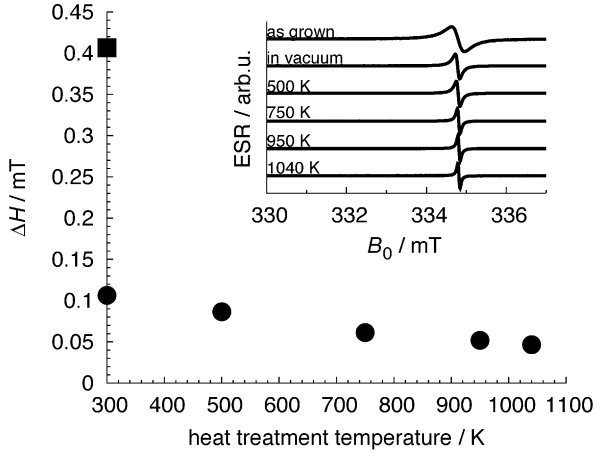

Figure 7. Evolution of the ESR line width, ΔH, at $T=300$ K, and $\nu=9.4$ GHz of samples undergone various heat treatments under dynamic vacuum (●). ■ = The as-grown sample. Inset: ESR spectrum at $T=300$ K after subsequent heat treatments with the spectra normalized for comparison.

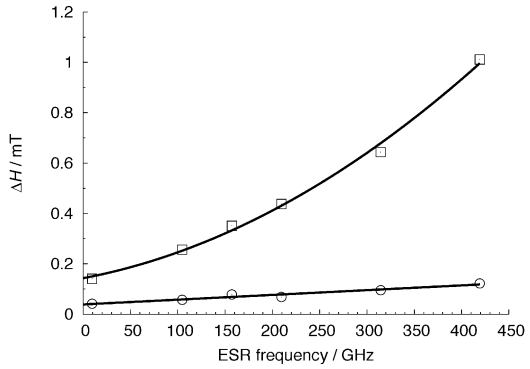

Figure 8. Frequency dependence of ΔH at $T=300$ K for a heat-treated graphene sample at 1040 K (○) demonstrating a linear increase in the line broadening with respect to frequency in the 0–420 GHz frequency range (0–16 T field range). The frequency dependence of the air-exposed graphene sample (□). Linear and quadratic lines of best fit (bottom and top, respectively) to line width broadening behavior are shown.[23]

a function of increasing heat treatment temperature. The intensity of the ESR line of a heat-treated sample under vacuum at 1040 K was approximately 25 times more intense than that of the as-prepared sample in an atmosphere of air; the spin concentration of the 1040 K heat-treated sample was found to be $\chi=3.7\times10^{19}$ spin g^{-1}. The resulting narrow ESR line indicated it was of carbon origin.

The chemical species responsible for the line width broadening were progressively removed by heating. Deviations from the Lorentzian line shape were also reduced (the Supporting Information, Figure S3.1 b). The ESR linewidth decreased to $\Delta H=0.046$ mT after heat treatment at 1040 K; this is an order of magnitude smaller than that observed in the as-prepared graphene exposed to air. The ESR line width narrowed approximately 6 times more as a result of dynamic vacuum pumping at 300 K (from 0.460 to 0.106 mT) than that from the subsequent heating to 1040 K (from 0.106 to 0.046 mT). The line width narrowing and intensity increase after heat treatment was reversible: Exposing the heat-treated samples to air resulted in an increase of the line width by an order of magnitude, and a decrease in the intensity. The as-grown ESR line was recovered upon venting the sample by air. We attribute this drastic change of T_S upon graphene exposure to air, to the interaction of graphene with the spin magnetic moments of O_2 in air.

Our earlier report showed that the ESR of chemically synthesized graphene is a common resonance of both localized and itinerant spins.[7] The conduction electron spin resonance in only observable below $\approx$50 K at high magnetic fields due to the small g-factor anisotropy.[7] However, the $\Delta H_{vac}=0.046$ mT line width of the 1040 K heat-treated sample at room temperature is significantly narrowed by itinerant conduction electrons.[7] To identify the contributions to motional narrowing made by conduction electrons we performed high-frequency ESR at $T=300$ K and analyzed the line width distortion relative to the Lorentzian profile on the 1040 K heat-treated sample (Figure 8 and the Supporting Information, Figure S3). In this experiment, we fixed the concentration of O_2 by sealing our sample under vacuum and an atmosphere of air, while tuning the ability of conduction electrons to narrow the signal motionally by varying the ESR frequency. Under these conditions the signal of the closed sample under vacuum broadened monotonically from $\Delta H_0=0.039$ mT residual width by a rate of 1.9×10^{-4} mT GHz^{-1} with increasing frequency.[7] Moreover, the magnitude of the non-Lorentzian residue also increased with increasing frequency (the Supporting Information, Figure S3). The low-pressure air closed sample behaves qualitatively similar (Figure 8). It shows $\Delta H_0=0.150$ mT, which is significantly broadened relative to the vacuum closed sample in accordance with the atmosphere dependence (Figure 7). In addition, the residual non-Lorentzian component of the sample closed under a low pressure of air was higher than that of the vacuum closed sample (Figure 7). However, the frequency dependence is quadratic with 3.3×10^{-6} mT GHz^{-2} coefficient rather than linear (Figure 8). All this is in agreement with an incomplete motional narrowing mechanism.[7]

The increasing deviation from the Lorentzian line shape with increasing frequency at a constant O_2 concentration demonstrated that conduction electrons were counter-balancing the spin depolarization induced by O_2 spins. Although the narrowing effect of the conduction electron is suppressed due to O_2 induced local magnetic field inhomogeneity, the narrowing strength is the same only it is less efficient.[23] The quadratic in the field dependence for the air-exposed sample indicates that the maximum experimentally available magnetic field, 16 T, is close to resolving the inhomogeneous signal.

When considering our results we propose that the broadening of the ESR line width, that is, the major reduction of the spin lifetime in graphene, results from the exposure to paramagnetic O_2 molecules in air and to a lesser extent the presence of covalently bonded oxygen groups on the graphene surface. Introducing less than 0.4 wt.% physisorbed O_2 broadened the ESR linewidth 6 times more than removing 18 wt.% of covalently bound oxygen as O–C or O=C (as determined by XPS). Assuming only magnetic dipole–dipole interac-

tion as a microscopic origin of the ESR line width broadening, average carbon–O_2 distances can be obtained: By fixing the electron spin $S=1/2$ to carbon and $S=1$ to an extrinsic spin (in our case O_2, since H_2O, N_2, and CO_2 are all in a ground electronic singlet state of $S=0$), the average distance between graphene–O_2 spins is obtained by the Van Vlack formula.[24] The closest value to the intrinsic homogeneous line width of our graphene sample was $\Delta H_{vac}=0.046$ mT, which results in a remarkably long spin lifetime, T_S, of 140 ns. This yields greater than $\approx$2.5 nm carbon–O_2 distances otherwise dipole–dipole interactions would readily broaden the spectral lines. This signal originates from regions in which carbon spins are protected from interacting with O_2 therefore pose the longest electron spin lifetimes.

There is an instrumental noise floor limiting ΔH detection of about 1 mT in the present experiment which translates to $\approx$1.1 nm distance. This is because ESR can only detect regions in which the line width is sufficiently narrow, as the signal amplitude is inversely proportional to the square of the line width.[13] Hence, in regions in which O_2 and graphene electron spins are separated by less than $\approx$1.1 nm, an ESR signal would not be observed in our experiments. This is the origin of the loss of the ESR signal upon O_2 exposure. However, the partial loss of ESR signal upon O_2 exposure observed in our experiments is a drastic consequence of O_2 inhomogeneity within the graphene sample. The residual non-Lorentzian intensity we observe in the Supporting Information (Figures S3.1 and S3.2) also indicates the broadening of the ESR line width by O_2 occurs irregularly throughout the sample; there are regions where barriers exist on the surface on graphene that may impede O_2 homogeneity, which includes other adsorbed molecules blocking the surface (e.g., H_2O), chemical reaction, and the extended porous graphene network itself. The maximum observed O_2 induced broadening of the ESR line width by $\approx$0.4 mT corresponded to a reduction of T_S to 16 ns. This yields about 1.4 nm carbon–O_2 spin distance. This discussion can hence be formulated in two ways: a) $\approx$4% of the total as-prepared sample volume consists of carbon spins separated from O_2 by a distance greater than 2.5 nm, or b) $\approx$96% of this sample volume is exposed to O_2 in a way that the carbon–O_2 distance is shorter than 1.1 nm. A schematic to represent the possible mechanism is presented in Figure 9.

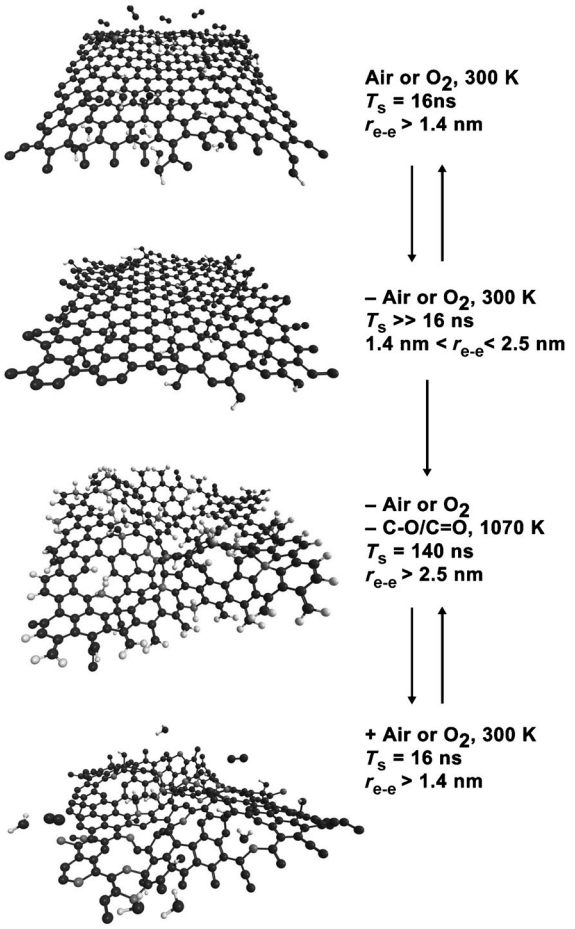

Figure 9. Schematic representation summarizing the effect of bound oxygen molecules on the surface of graphene. The average spin-spin distance is denoted by r_{e-e}. Hydrogen has been omitted in certain graphene fragment models for clarity. After the removal of molecules from air (or removal of O_2) at 300 K the spin lifetime increases, with only the covalently bound oxygen remaining on the graphene. Further heating removes covalent-bound oxygen, further increasing the spin lifetime in graphene. Re-exposing the heated graphene material to air (or O_2) introduces adsorbed molecules, although oxidation is very slow and irreversible. In both the as-synthesized and heat-treated samples, this exposure to O_2 or air causes a drastic reduction in the observed spin lifetime.

4. Conclusions

By multifrequency ESR we have demonstrated that removing both chemisorbed and physisorbed oxygen on graphene decreases the observed ESR line width, which physically translates to an increase in electron spin lifetime. Removal of covalently bound oxygen groups is largely irreversible; however, the adsorption of O_2 on the graphene surface was sufficient to completely revert to the short spin lifetimes. As paramagnetic O_2 spin centers are introduced, they rapidly physisorb to the graphene surface while taking an exceptionally long time to equilibrate throughout the entire porous graphene material. Exposure of the graphene sample to air also introduces considerable amounts of H_2O, and to a lesser extent N_2 and CO_2. This also contributes to inhomogeneity in the spread of oxygen–carbon spin interactions across various regions of the graphene surface individually distinguished by ESR. Dipole–dipole interactions between the graphene surface and localized paramagnetic oxygen spins destroys spin coherence, which manifests as an increase in the observed ESR line width. The closer the paramagnetic oxygen centers are to the graphene surface the shorter the observed electron spin lifetime; at distances closer than $\approx$1.4 nm the electron spin lifetime is reduced beyond detection by ESR. When oxygen and carbon spin centers are separated beyond $\approx$2.4 nm, we are able to observe the intrinsic extraordinarily long electron spin lifetime in our graphene material (localized spin, 140 ns) which makes it of exceptional quality for potential use in assembling spintronic devices (N.B., conduction electron spin, $T_S=65$ ns). The mechanisms by which various covalently bound oxygen

groups on graphene influence spin lifetime remain unclear. Given the sensitivity to oxygen molecules a few nanometers away, future attempts to assemble graphene-based spintronic devices will require the special consideration of surrounding chemical environments.

Acknowledgements

M.C. acknowledges financial assistance from the University of Sydney. Work at Lausanne was supported by the Swiss National Science Foundation.

Keywords: gas adsorption · graphene · oxygen · spintronics · surface chemistry

[1] a) R. G. Mani, J. Hankinson, C. Berger, W. A. de Heer, *Nat. Commun.* **2012**, *3*, 996; b) W. Han, K. Pi, K. M. McCreary, Y. Li, J. J. I. Wong, A. G. Swartz, R. K. Kawakami, *Phys. Rev. Lett.* **2010**, *105*, 167202; c) N. Tombros, C. Jozsa, M. Popinciuc, H. T. Jonkman, B. J. van Wees, *Nature* **2007**, *448*, 571 – 574; d) T. Y. Yang, J. Balakrishnan, F. Volmer, A. Avsar, M. Jaiswal, J. Samm, S. R. Ali, A. Pachoud, M. Zeng, M. Popinciuc, G. Güntherodt, B. Beschoten, B. Özyilmaz, *Phys. Rev. Lett.* **2011**, *107*, 047206.

[2] a) T. Jayasekera, B. D. Kong, K. W. Kim, M. Buongiorno Nardelli, *Phys. Rev. Lett.* **2010**, *104*, 146801; b) S. Krompiewski, *Nanotechnology* **2012**, *23*, 135203.

[3] M. Gmitra, S. Konschuh, C. Ertler, C. Ambrosch-Draxl, J. Fabian, *Phys. Rev. B* **2009**, *80*, 235431.

[4] a) A. H. Castro Neto, F. Guinea, *Phys. Rev. Lett.* **2009**, *103*, 026804; b) C. Józsa, T. Maassen, M. Popinciuc, P. J. Zomer, A. Veligura, H. T. Jonkman, B. J. van Wees, *Phys. Rev. B* **2009**, *80*, 241403.

[5] a) W. H. Wang, K. Pi, Y. Li, Y. F. Chiang, P. Wei, J. Shi, R. K. Kawakami, *Phys. Rev. B* **2008**, *77*, 020402; b) M. Popinciuc, C. Józsa, P. J. Zomer, N. Tombros, A. Veligura, H. T. Jonkman, B. J. van Wees, *Phys. Rev. B* **2009**, *80*, 214427.

[6] a) L. Tapasztó, T. Dumitrică, S. J. Kim, P. Nemes-Incze, C. Hwang, L. P. Biró, *Nature Phys. Sci.* **2012**, *8*, 739 – 742; b) V. K. Dugaev, E. Y. Sherman, J. Barnaś, *Phys. Rev. B* **2011**, *83*, 085306; c) D. Huertas-Hernando, F. Guinea, A. Brataas, *Phys. Rev. Lett.* **2009**, *103*, 146801.

[7] B. Náfrádi, M. Choucair, L. Forró, *Carbon* **2014**, *74*, 346 – 351.

[8] a) M. Choucair, P. Thordarson, J. A. Stride, *Nat. Nanotechnol.* **2009**, *4*, 30 – 33; b) M. Choucair, N. M. K. Tse, M. R. Hill, J. A. Stride, *Surf. Sci.* **2012**, *606*, 34 – 39.

[9] a) M. A. Augustyniak-Jabłokow, K. Tadyszak, M. Maćkowiak, S. Lijewski, *Chem. Phys. Lett.* **2013**, *557*, 118 – 122; b) S. Ishii, K. Miyamoto, N. Oguri, K. Horiuchi, T. Sasaki, N. Aoki, Y. Ochiai, *Phys. E* **2003**, *19*, 149 – 152; c) S. S. Rao, A. Stesmans, J. van Tol, D. V. Kosynkin, A. Higginbotham-Duque, W. Lu, A. Sinitskii, J. M. Tour, *ACS Nano* **2012**, *6*, 7615 – 7623; d) L. Ćirić, A. Sienkiewicz, D. M. Djokić, R. Smajda, A. Magrez, T. Kaspar, R. Nesper, L. Forró, *Phys. Status Solidi B* **2010**, *247*, 2958 – 2961; e) G. Wagoner, *Phys. Rev.* **1960**, *118*, 647 – 653; f) L. Ćirić, A. Sienkiewicz, B. Náfrádi, M. Mionić, A. Magrez, L. Forró, *Phys. Status Solidi B* **2009**, *246*, 2558 – 2561; g) B. Náfrádi, N. M. Nemes, T. Fehér, L. Forró, Y. Kim, J. E. Fischer, D. E. Luzzi, F. Simon, H. Kuzmany, *Phys. Status Solidi B* **2006**, *243*, 3106 – 3110; h) P. Szirmai, G. Fábián, J. Koltai, B. Náfrádi, L. Forró, T. Pichler, O. A. Williams, S. Mandal, C. Bäuerle, F. Simon, *Phys. Rev. B* **2013**, *87*, 195132; i) F. Simon, H. Kuzmany, B. Náfrádi, T. Fehér, L. Forró, F. Fülöp, A. Jánossy, L. Korecz, A. Rockenbauer, F. Hauke, A. Hirsch, *Phys. Rev. Lett.* **2006**, *97*, 136801; j) S. Tóth, D. Quintavalle, B. Náfrádi, L. Korecz, L. Forró, F. Simon, *Phys. Rev. B* **2008**, *77*, 214409.

[10] a) K. L. Nagy, B. Náfrádi, N. D. Kushch, E. B. Yagubskii, E. Herdtweck, T. Fehér, L. F. Kiss, L. Forró, A. Jánossy, *Phys. Rev. B* **2009**, *80*, 104407; b) Á. Antal, T. Fehér, E. Tátrai-Szekeres, F. Fülöp, B. Náfrádi, L. Forró, A. Jánossy, *Phys. Rev. B* **2011**, *84*, 075124; c) Á. Antal, T. Fehér, B. Náfrádi, R. Gaál, L. Forró, A. Jánossy, *Physica B* **2010**, *405*, S168 – S171.

[11] a) C. F. M. Clewett, P. Li, T. Pietrass, *J. Phys. Chem. C* **2007**, *111*, 6263 – 6267; b) V. L. J. Joly, M. Kiguchi, S.-J. Hao, K. Takai, T. Enoki, R. Sumii, K. Amemiya, H. Muramatsu, T. Hayashi, Y. A. Kim, M. Endo, J. Campos-Delgado, F. López-Urías, A. Botello-Méndez, H. Terrones, M. Terrones, M. S. Dresselhaus, *Phys. Rev. B* **2010**, *81*, 245428; c) S. S. Rao, A. Stesmans, K. Keunen, D. V. Kosynkin, A. Higginbotham, J. M. Tour, *Appl. Phys. Lett.* **2011**, *98*, 083116 – 083113.

[12] a) B. Náfrádi, R. Gaál, T. Fehér, L. Forró, *J. Magn. Reson.* **2008**, *192*, 265 – 268; b) B. Náfrádi, R. Gaál, A. Sienkiewicz, T. Fehér, L. Forró, *J. Magn. Reson.* **2008**, *195*, 206 – 210.

[13] P. Szirmai, G. Fábián, B. Dóra, J. Koltai, V. Zólyomi, J. Kürti, N. M. Nemes, L. Forró, F. Simon, *Phys. Status Solidi B* **2011**, *248*, 2688 – 2691.

[14] A. Abragam, B. Bleaney, *Electron Paramagnetic Resonance of Transition Ions*, Oxford University Press, Oxford, **1970**.

[15] A. C. Ferrari, J. Robertson, *Phys. Rev. B* **2000**, *61*, 14095 – 14107.

[16] A. C. Ferrari, D. M. Basko, *Nat. Nanotechnol.* **2013**, *8*, 235 – 246.

[17] L. G. Cançado, A. Jorio, E. H. M. Ferreira, F. Stavale, C. A. Achete, R. B. Capaz, M. V. O. Moutinho, A. Lombardo, T. S. Kulmala, A. C. Ferrari, *Nano Lett.* **2011**, *11*, 3190 – 3196.

[18] C. Casiraghi, S. Pisana, K. S. Novoselov, A. K. Geim, A. C. Ferrari, *Appl. Phys. Lett.* **2007**, *91*, 233108.

[19] a) T. M. G. Mohiuddin, A. Lombardo, R. R. Nair, A. Bonetti, G. Savini, R. Jalil, N. Bonini, D. M. Basko, C. Galiotis, N. Marzari, K. S. Novoselov, A. K. Geim, A. C. Ferrari, *Phys. Rev. B* **2009**, *79*, 205433; b) J. E. Proctor, E. Gregoryanz, K. S. Novoselov, M. Lotya, J. N. Coleman, M. P. Halsall, *Phys. Rev. B* **2009**, *80*, 073408.

[20] a) S. Sircar, J. R. Hufton, *Adsorption* **2000**, *6*, 137 – 147; b) E. Glueckauf, J. I. Coates, *J. Chem. Soc.* **1947**, 1315 – 1321.

[21] J. Stankowski, S. Waplak, W. Bednarski, *Solid State Commun.* **2000**, *115*, 489 – 491.

[22] a) B. Náfrádi, A. Olariu, L. Forró, C. Mézière, P. Batail, A. Jánossy, *Phys. Rev. B* **2010**, *81*, 224438; b) Á. Antal, A. Jánossy, L. Forró, E. J. M. Vertelman, P. J. van Koningsbruggen, P. H. M. van Loosdrecht, *Phys. Rev. B* **2010**, *82*, 014422.

[23] P. W. Anderson, *J. Phys. Soc. Jpn.* **1954**, *9*, 316 – 339.

[24] J. H. Van Vleck, *Phys. Rev.* **1948**, *74*, 1168 – 1183.

Received: July 9, 2014
Published online on November 13, 2014